Journal of Applied Electrochemistry
https://doi.org/10.1007/s10800-021-01585-7

RESEARCH ARTICLE

Polymer-metal complexes as emerging catalysts for electrochemical reduction of carbon dioxide

Daniele Sassone[1,2] · Juqin Zeng[1] · Marco Fontana[1] · Adriano Sacco[1] · M. Amin Farkhondehfal[1] · Monica Periolatto[2] · Candido F. Pirri[1,2] · Sergio Bocchini[1]

Received: 16 January 2021 / Accepted: 31 May 2021

Abstract

A class of metal-doped polyanilines (PANIs) was synthesized and investigated as electrocatalysts for the carbon dioxide reduction reaction (CO_2RR). These materials show good affinity for the electrode substrate and allow to obtain stable binder-free electrodes, avoiding the utilization of expensive ionomer and additives. The emeraldine-base polyaniline (EB-PANI), in absence of metal dopant, shows negligible electrocatalytic activity and selectivity toward the CO_2RR. Such behavior significantly improves once EB-PANI is doped with an appropriate cationic metal (Mn, Cu or Sn). In particular, the Sn-PANI outperforms other metal-doped samples, showing a good turnover frequency of 72.2 h^{-1} for the CO_2RR at − 0.99 V vs the reversible hydrogen electrode and thus satisfactory activity of metal single atoms. Moreover, the Sn-PANI also displays impressive stability with a 100% retention of the CO_2RR selectivity and an enhanced current density of 4.0 mA cm^{-2} in a 10-h test. PANI, a relatively low-cost substrate, demonstrates to be easily complexed with different metal cations and thus shows high tailorability. Complexing metal with conductive polymer represents an emerging strategy to realize active and stable metal single-atom catalysts, allowing efficient utilization of metals, especially the raw and precious ones.

Graphic abstract

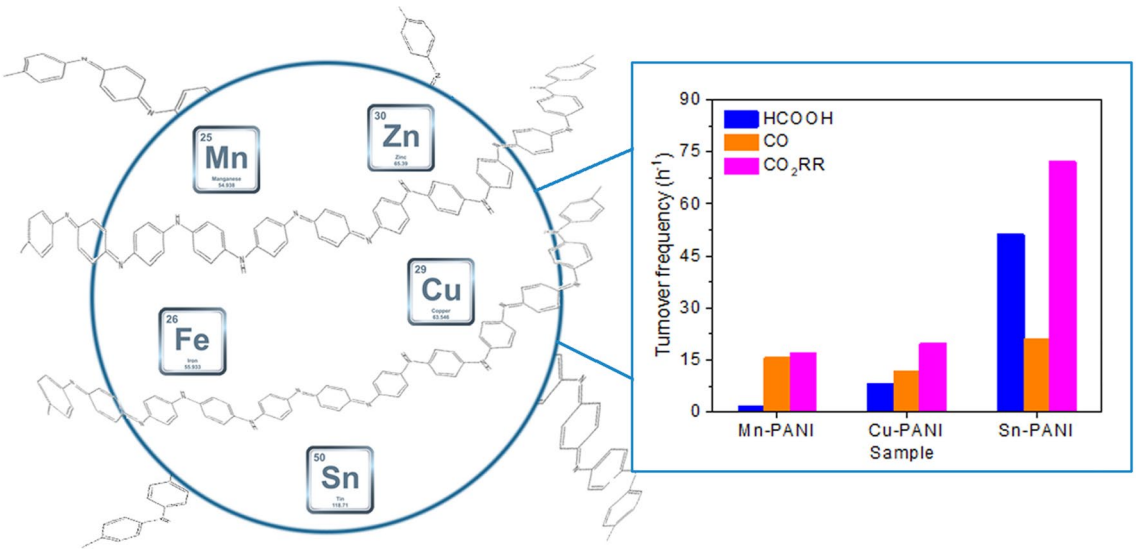

Keywords Carbon dioxide reduction · Electrocatalysis · Polyaniline · Single-atom catalysts · Stability

✉ Juqin Zeng
juqin.zeng@iit.it

Extended author information available on the last page of the article

Published online: 21 June 2021

1 Introduction

Energy consumption rapidly grows all around the world, from emerging countries with conventional industries to western society with more and more sophisticated technologies, demanding fast increase in the fossil fuels combustion and consequently boosting the CO_2 emission. Conversion of CO_2 into valuable chemicals and fuels is supposed to bring benefits not only to the climate and natural carbon cycle, but also to the long-term energy storage for confronting the future fossil fuel shortage [1]. Among many technologies, the electrochemical process is of great interest since it can be conducted at mild conditions using excess electricity from the grid as energy input and the products are highly tunable by utilizing different catalysts and applying various potentials. Although being very promising, the electrochemical CO_2 conversion confronts many challenges due to the high energy barriers, slow kinetics and complex pathways of the CO_2 reduction reaction (CO_2RR). Hence, rationally designed electrocatalysts are essential to advance this technology. An ideal electrocatalyst should have high activity, good selectivity toward specific products and satisfactory stability over long-time operation. Among numerous investigated metallic electrodes [2], copper nanoparticles are uniquely able to produce C_2 and C_3 molecules [3–5]; silver, gold and zinc show the best selectivity for CO production [6–8]; p-block metals (In, Sn, Pb) are selective catalysts for the $HCOOH/HCOO^-$ formation [9]. Significant improvements can be reached switching from mono-metal systems to rationally designed multi-metal alloys taking advantage of the synergistic effect of different metals [10–12]. Despite the promising performance, a general limit of metallic electrodes is the high price and the scarce availability of many chemical species. These materials, even in the form of nanostructures, have low active sites-to-mass ratios. Hence, it could be of vital importance to increase the utilization efficiency of the metal, especially considering that many metals are critical raw materials due to limited availability, geopolitical conflicts in the source's countries, toxicity and other factors [13]. In order to enhance the metal utilization, an ideal strategy is to constrain each single metal atom to act as active site for the reaction [14–17]. From this perspective, organometallic complexes are the best example, in which each metal cation/atom coordinates different ligands, being stabilized and enriched in electron density [18]. Those molecules are commonly used in homogeneous catalysis systems that require the catalyst dissolution in a proper solvent without being immobilized onto the working electrode. Even though high turnover number and turnover frequency values are reported, the stability of this class of molecules is often discouraging [19]. In addition, high overpotentials could be required to form the active catalytic species and to overcome the low conductivity.

This work aims at obtaining metal single-atom catalysts with a high active sites-to-metal ratio, possessing satisfactory activity, selectivity and stability in the CO_2RR. Polyaniline (PANI) has been widely studied as a support for metal nanoparticles like Cu, Pd and Pt [20, 21], and also as a precursor for nitrogen-doped carbon materials synthesized through a pyrolysis process [22, 23]. However, it has never been investigated itself as electrocatalyst for the CO_2RR. It is known to be semiconductive in the non-protonated form (emeraldine base, EB-PANI) and conductive in the emeraldine protonated form (emeraldine salt, ES-PANI) [24]. The conductive PANI can also be obtained through the use of Lewis acids such as metal cations [25]. In the present work, EB-PANI and PANIs doped with various metal cations (Mn, Cu, Sn and Fe ions) were synthesized and investigated for the first time as heterogeneous catalysts for the CO_2RR, combining the single metal atom activity typical of the homogenous molecular catalysis with the good stability of the heterogeneous catalysts.

2 Experimental section

2.1 Chemicals and materials

All reagents were purchased from commercial sources without further purification. N-phenyl-1,4-phenylenediamine (DANI, 98%), copper (II) chloride ($CuCl_2$, 99%), iron (III) chloride ($FeCl_3{\cdot}6H_2O$, 97%), manganese (II) chloride ($MnCl_2$, 99%), tin (IV) chloride ($SnCl_4{\cdot}5H_2O$, 98%) ammoniumpersulfate (APS, $(NH_4)_2S_2O_8$, 98%), methanol (MeOH, 99.9%), N-methyl-2-pyrrolidinone (NMP, 99.5%), hydrochloric acid fuming (HCl, 37%), potassium bromide (KBr, 99%), Nafion™ 117 containing solution (5% in a mixture of lower aliphatic alcohols and water) were all purchased from Merck.

2.2 Synthesis

The ES-PANI was synthetized by bulk polymerization using DANI (5 gr, 27.1 mmol) as monomer and APS (9.29 gr, 40.7 mmol) as oxidizing agent in 20 mL of solution 70:30 v/v MeOH:H_2O with 1% w/w of HCl. DANI was dissolved in 15 mL of the starting solution and placed in an ice bath under stirring, while APS was dissolved in the remaining 5 mL of the starting solution. Then, the APS solution was slowly added dropwise into the DANI solution in 5 min and kept under stirring for 3 h at room temperature (RT). The obtained dark green precipitate was filtered, washed several times with a solution 70:30 MeOH:H_2O (in order to dissolve the low molecular

weight polymers) and then dried at 60 °C. In order to obtain EB-PANI, the powder was dispersed in 40 mL of ammonia 32% solution and stirred overnight, then filtered and washed with water several times and dried overnight at 60 °C. Doping reaction was performed dissolving 100 mg (around 1 mmol) of EB-PANI and 11 mmol of the relative metal salt ($MnCl_2$, $CuCl_2$, $SnCl_4{\cdot}6H_2O$ or $FeCl_3$) in 20 mL of MeOH and stirred at 60 °C overnight. The solution was then diluted in water to promote the metal-PANI precipitation. The obtained precipitate was thus filtered, washed several times with water in order to remove any residual trace salts, and then dried overnight at 60 °C.

2.3 Physical and chemical characterizations

Fourier-transform infrared spectroscopy (FT-IR) analysis was performed using KBr pellets on a Bruker Tensor II in transmission mode. The pellets were prepared grinding 1 mg of sample with 200 mg of anhydrous KBr and then compacting with a pressure of 10 ton cm^{-1}.

Inductively coupled plasma-mass spectroscopy (ICP-MS) analysis was performed on an Icap Q ICP-MS (Thermo Fisher) and the data were collected and processed by the related Thermo Fischer ICP software.

UV–Vis spectroscopy was performed with a Perkin-Helmer UV/Vis/NIR spectrometer LAMBDA™ 650 S in absorption mode. Each sample (1 mg) was dissolved in NMP (5 mL) to prepare the solution. Blank solvent spectrum was subtracted from each recorded spectrum.

Field-emission scanning electron microscopy (FESEM) characterization was performed on a ZEISS Supra 40 FESEM microscope.

X-ray photoelectron spectroscopy (XPS) analysis was performed with a PHI 5000 Versaprobe spectrometer (Physical Electronics), equipped with monochromatic Al K-alpha X-ray source (1486.6 eV). Surface charge compensation was obtained with a combined system, based on an electron gun and Ar^+ ion gun. Survey and high-resolution (HR) spectra were acquired using pass energy (PE) values of 187.85 and 23.50 eV, respectively. The calibration of the binding energy (BE) scale was obtained by setting the C–C sp^2 component of the C 1 s region to 284.5 eV. Casa XPS software was used for the analysis of the experimental data. The Shirley background function was subtracted from HR spectra to remove the background signal [26]. The reported uncertainties on relative atomic concentrations were calculated with Monte Carlo routines implemented in Casa XPS.

2.4 Electrochemical characterization

2.4.1 Preparation of electrodes

The as-prepared catalysts were coated onto a carbon paper (gas diffusion layer, GDL; SIGRACET 28BC, SGL Technologies) to obtain electrodes. To prepare a binder-free electrode, 1 mg of catalyst (EB-PANI, Cu-PANI, Sn-PANI, Mn-PANI or Fe-PANI) was dispersed in 160 µL of ethanol by sonication. The obtained uniform slurry was then drop-casted on the GDL and dried in air overnight. Each electrode has a catalyst loading of 0.7 mg cm^{-2}. To study the composition effect on the CO_2RR, four Cu-PANI electrodes with various compositions were prepared: (i) a free-standing one with only catalyst, (ii) a second one with the addition of 0.3 mg of carbon black (CB, Shawinigan Black AB50), (iii) a third one with the addition of 40 µL of Nafion solution (Nafion® 117 solution, 5 wt. %) and (iv) the last one with the addition of both CB (0.3 mg) and Nafion solution (40 µL).

2.4.2 Cyclic voltammetry (CV) and electrochemical impedance spectroscopy (EIS)

The electrochemical characterization was firstly performed through CV and EIS in a three-electrode H-type cell at RT with a Metrohm Multi Autolab/M101 potentiostat. The working electrode was a catalyst-coated carbon paper with a geometric area of 0.15 cm^2. A Pt wire was used as counter electrode and an Ag/AgCl (3 M NaCl) was used as reference electrode. A membrane (Nafion™ Membrane N117, Sigma-Aldrich) was employed to separate the cathodic and anodic compartments. CV measurements were performed from 0.73 to − 1.07 V vs Reference Hydrogen Electrode (RHE) at a scan rate of 10 mV s^{-1} in N_2- and CO_2-saturated/purged (5 mL min^{-1}) 0.1 M $KHCO_3$ aqueous solution. Unless otherwise specified, all the potentials refer to RHE in this work. The potential applied versus Ag/AgCl was converted to that versus RHE using the formula E (vs RHE) = E (vs Ag/AgCl) + 0.197 V + 0.0591 × pH. To determine the double-layer capacitance of the electrode, CV was executed in a potential range of − 0.24 V to − 0.39 V at scan rates of 2 mV s^{-1}, 5 mV s^{-1}, 10 mV s^{-1}, 25 mV s^{-1}, 50 mV s^{-1}, 75 mV s^{-1} and 100 mV s^{-1} in the N_2-saturated 0.1 M $KHCO_3$ aqueous solution. EIS measurements were performed at various potentials from − 0.19 V to − 0.99 V with an AC signal of 10 mV of amplitude and 1–10^5 Hz frequency range in N_2- and CO_2-saturated 0.1 M $KHCO_3$ aqueous solutions.

2.4.3 Chronoamperometric (CA) measurement and product analysis

CA tests were performed with a CHI 760D (CH Instruments, Inc.) potentiostat in a customized H-type EC cell (Electro-Cell™, Scheme S1) in order to study the CO_2RR and to quantify the products. A catalyst-coated carbon paper of 1.5 cm^2 was used as the working electrode, a platinum foil as the counter and an Ag/AgCl (1 mm, leak-free LF-1) as the reference. Gas-phase products were analyzed on-line by a micro gas chromatograph (μGC, Fusion®, INFICON) with two channels containing a 10 m Rt-Molsieve 5A column and an 8 m Rt–Q–Bond column, respectively. Both channels are equipped with a micro thermal conductivity detector (micro-TCD). The inlet of the μGC equipment was connected to the cathodic side of the electrochemical cell through a GENIE filter to remove the humidity from the gas. During the CA measurements, a constant CO_2 flow rate of 10 mL min^{-1} was maintained to saturate the electrolyte and to carry out the gaseous products to the μGC. Liquid products were analyzed by a High-Performance Liquid Chromatograph (Thermo Scientific Ultimate3000 HPLC) with a UV–Vis Detector set at 210 nm using a ReproGel (300 × 8 mm) column, with 9.0 mM H_2SO_4 (flow rate of 1.0 mL min^{-1}) as mobile phase. The faradaic efficiency (FE) for each product was calculated by dividing the coulombs needed to produce the actual determined amount of this product by the total coulombs consumed during a corresponding reduction period.

3 Results and discussion

3.1 Physical and chemical properties of the samples

FT-IR was performed to study the correct polymerization of EB-PANI and metal-doped PANI samples. A typical absorption pattern of polyaniline is observed for the ES-PANI (Figure S1) and it is preserved for the EB-PANI and metal-doped samples (Fig. 1). EB-PANI shows the characteristic ν_{N-H} at 3172 cm^{-1} stretching of secondary amines, the ν_{C-H} at 3031 cm^{-1} stretching of aromatic rings, the ν_{C-N} at 1597 cm^{-1} of the benzenoid ring and the ν_{C-C} at 1495 cm^{-1} stretching of the quinoid ring of the polymer chain, the ν_{C-N} at 1312 cm^{-1} stretching of aromatic amines, the quinoid ring stretching at 1151 cm^{-1}, and the out of plane bending of para-disubstituted benzene at 819 cm^{-1}. Similar patterns are recorded for the metal-doped PANI samples, indicating good preservation of the polymer chains during the doping reaction.

Successful incorporation of metal elements is confirmed by ICP-MS and XPS analysis. Figure S2 reports representative survey spectra for all the analyzed samples, alongside labels for the most intense peaks related to the detected

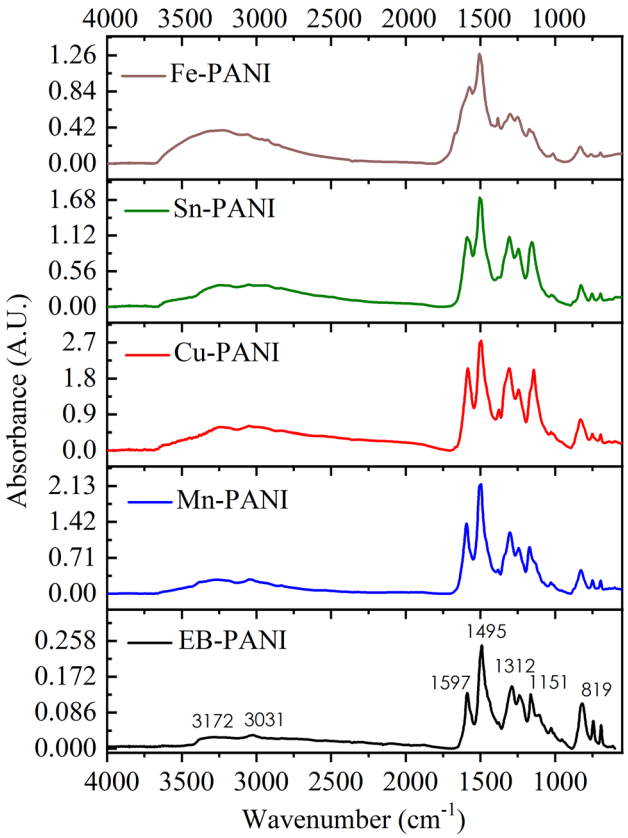

Fig. 1 FT-IR spectra of EB-PANI and metal-doped PANI samples

chemical elements. The weight percentage of doped metal and the atomic ratio of metal to coordinated nitrogen were quantified and listed in Table 1. It is confirmed that the chemical composition of the synthesized EB-PANI is in accordance with the reported molecular structure [27, 28], alongside slight oxidation and residual chlorine content from the polymerization process.

High-resolution XPS studies further provide information on the oxidation state of the metal cations. For Cu-PANI sample (Fig. 2a), the $Cu2p_{3/2}$ peak can be deconvoluted into two main contributions at 932.6 eV (75.6% peak area) and 934.6 eV (24.4% peak area), which can be attributed to Cu(I) and Cu(II), respectively, in accordance with the literature on CuCl [29], $CuCl_2$ [30] and Cu-doped polyaniline [31]. Based on the $Sn3d_{5/2}$ peak position (487.3 eV), it is possible to exclude the presence of metallic Sn in the Sn-PANI sample (Fig. 2b), while it is difficult to define the exact oxidation state (IV or II) of the Sn cations, due to the low sensitivity of the binding energy on the oxidation state of Sn [32]. Concerning the Mn-PANI sample (Fig. 2c), the identification of the oxidation state of Mn is not straightforward due to its low concentration and the well-known complexity of interpretation of the Mn2p region caused by multiplet-splitting and satellite structure [33]. Based on the estimated

Table 1 Metal percentage by ICP quantification and chemical composition by semi-quantitative high-resolution XPS analysis

Sample	ICP	XPS[a]					
	Metal (wt%)	C (at%)	O (at%)	N (at%)	Cl (at%)	Metal (at%)	Metal/N (at%/at%)
EB-PANI	/	80.5 (4) ± 0.4	3.9 (2) ± 0.2	15.2 (4) ± 0.4	0.4 (1) ± 0.1	/	/
Cu-PANI	8.9 ± 1.6	78.3 (7) ± 1.1	6.2 (3) ± 0.3	12.3 (6) ± 1.2	2.5 (1) ± 0.1	0.7 (1) ± 0.1	0.06 (1)
Sn-PANI	6.6 ± 1.1	71.5 (5) ± 0.5	9.8 (3) ± 0.3	11.2 (5) ± 0.5	4.7 (1) ± 0.1	2.8 (1) ± 0.1	0.25 (1)
Mn-PANI	2.2 ± 1.0	80.1 (4) ± 0.5	5.0 (2) ± 0.2	12.9 (5) ± 0.5	1.5 (1) ± 0.1	0.5 (1) ± 0.1	0.04 (1)
Fe-PANI	1.4 ± 1.0	72.0 (4) ± 0.5	13.8 (2) ± 0.2	8.6 (3) ± 0.5	4.6 (1) ± 0.1	1.1 (1) ± 0.1	0.13 (1)

a The uncertainties on the relative atomic concentrations are reported in brackets and they refer to the last digit

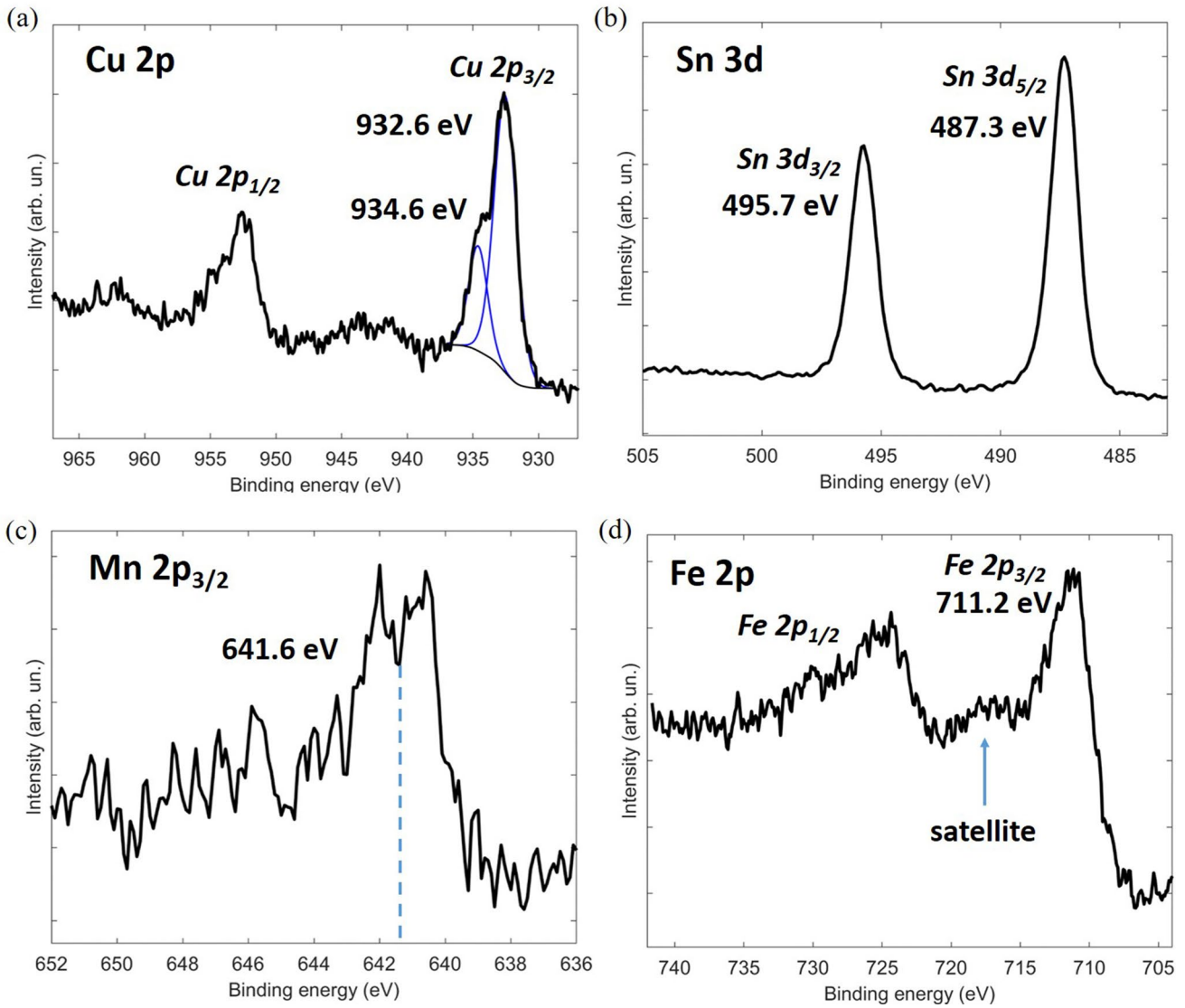

Fig. 2 High-resolution XPS acquisitions of the Cu2p, Sn3d, $Mn2p_{3/2}$ and Fe2p regions for samples **a** Cu-PANI, **b** Sn-PANI, **c** Mn-PANI and **d** Fe-PANI

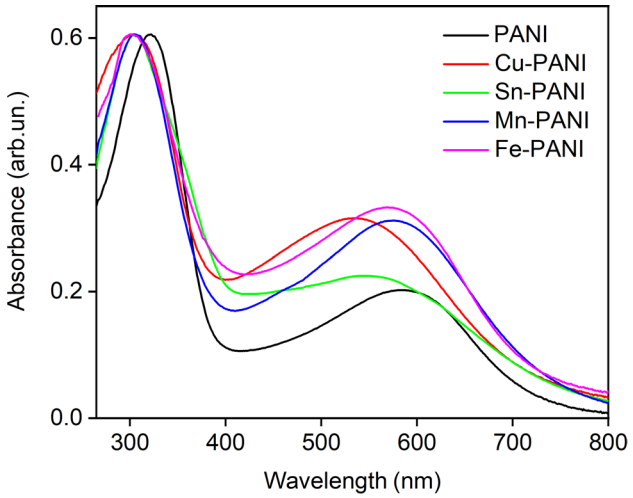

Fig. 3 Normalized UV–Vis spectra of PANI-based samples dissolved in NMP solution

binding energy of the $Mn2p_{3/2}$ peak (641.6 eV), the presence of Mn(III) and Mn(IV) seems most probable [34]. Regarding the Fe-PANI sample (Fig. 2d), both the $Fe2p_{3/2}$ peak at a binding energy of 711.2 eV and the presence of characteristic satellite, point to Fe(III), in accordance with the literature on $FeCl_3$ [35] and Fe-doped polyaniline [36]. Concisely, detailed XPS analysis unveils that Cu, Sn, Mn and Fe ions are successfully introduced in the EB-PANI as coordinated ions.

The UV–Vis spectra of various samples, normalized based on the as-obtained data, are shown in Fig. 3. Two transitions, the π-π* between 300 and 400 nm associated with the benzoid moiety absorption, and the π-polaron between 500 and 700 nm related to the bipolar formation, are present for EB-PANI. The spectra of metal-doped samples resemble the one recorded for EB-PANI, in agreement with the literature [37]. The absorption peaks are slightly different for each sample: 322 nm (π-π*) and 585 nm (π-polaron) for EB-PANI, 305 nm and 534 nm for Cu-PANI, 305 nm and 548 nm for Sn-PANI, 305 nm and 574 nm for Mn-PANI, 300 nm and 569 nm for Fe-PANI. It is interesting to note that the presence of metal cations leads to a hypsochromic shift (blue shift) for both π-π* and π-polaron transitions and causes an increase in the π-polaron absorption, evidencing that a doping process is involved at different scales for each cations [38]. The presence of cations indicates the formation of a metal complex and its chemical composition is influenced by the anion specie of the metal precursor. In the case of halogen metals, the anion is still present in the metal complex as halogen ligand due to its favorable coordinative properties, as evidenced by XPS result (Table 1), while less coordinative anions such as nitrate could result in more complexation for the polyanilines [39].

Further study on the morphology has been performed by FESEM. As shown in Fig. 4, Sn-PANI preserves the morphology of EB-PANI without the presence of newly formed nanostructures. Similar morphology is also observed for Cu-, Mn- and Fe-PANI (Figure S3). This outcome indicates the successful doping of metal cations in the PANI matrix, in consistence with XPS and UV–Vis analysis.

3.2 Investigation of the electrode composition

To enable the electrochemical evaluation of the powder-like materials toward the CO_2RR, the as-prepared catalysts are usually coated onto a carbon paper to obtain the electrodes. In the literature, one commonly underestimated but crucial aspect is the composition of the electrode. Unlike in other research fields such as fuel cells, where the electrode composition has already been intensively studied, the investigation on the electrode fabrication for the CO_2RR is still not mature. In the literature, several methods are reported for the electrode preparation [40], while a specific study on the composition and the roles of each component is still missing. Generally, electrode fabrication requires a current collector that is usually a metal or carbon-based conductive substrate, a catalyst that is dispersed on the collector to maximize the accessibility, a binder that immobilizes the catalyst on the collector and other additives for

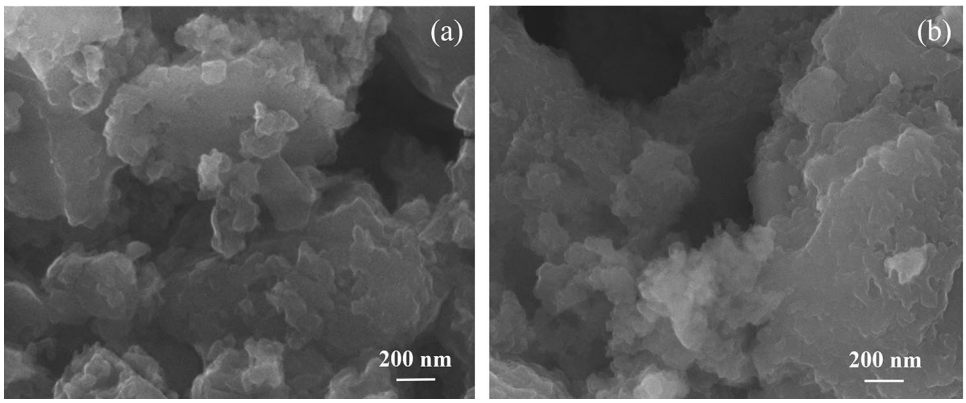

Fig. 4 FESEM images of **a** EB-PANI and **b** Sn-PANI

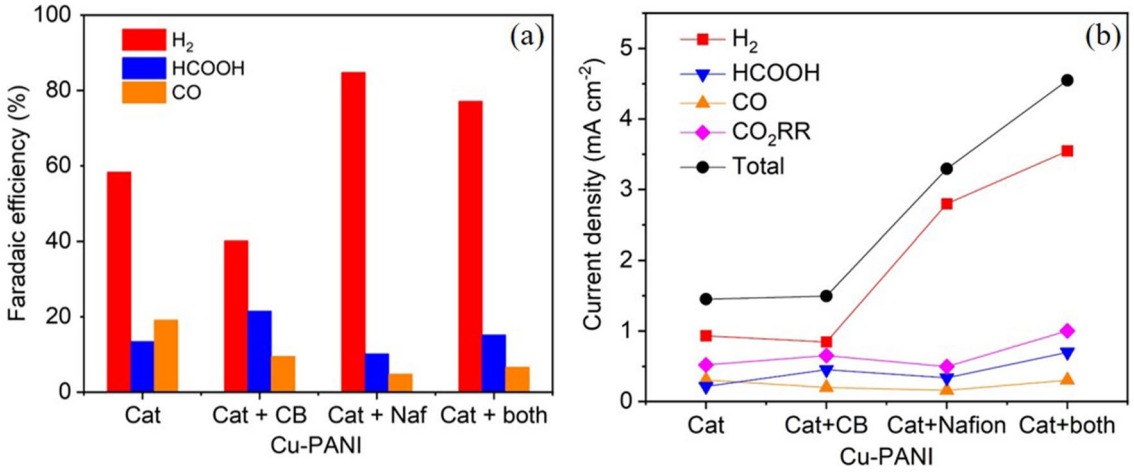

Fig. 5 CO_2RR on various electrodes with different compositions at − 0.99 V in CO_2-saturated 0.1 M $KHCO_3$ electrolyte: **a** Faradaic efficiencies and **b** partial current densities

enhancing the electrical contact or the ionic conductivity. In the CO_2RR, commercial carbon papers (equipped with GDL) are commonly used as the current collector and carbon blacks (CBs) are widely employed to enhance the electrical conductivity in the CO_2RR. Another commonly used additive is Nafion, an ionomer that acts both as a binder and as an ionic conductor. In order to study the effect of the individual components on the CO_2RR, we performed a cross investigation on various electrodes, including one containing only the catalyst (Cu-PANI), one containing Cu-PANI and CB, one containing Cu-PANI and Nafion, and a last one containing Cu-PANI, CB and Nafion, as shown in Fig. 5. Interestingly, Nafion addition dramatically favors the hydrogen evolution reaction (HER) in terms of both selectivity (higher FE_{H2}) and electrode activity (higher partial current density, j_{H2}), while it does not influence the electrode activity of the CO_2RR. It is believed that the fluorinated groups of the ionomer could increase the hydrophobicity of the electrode and promote the selectivity toward the reduction of CO_2 rather than protons [41]. However, the terminal chain sulfonic groups in Nafion lead to an increase in the overall surface polarity [27], resulting in the enhancement in the HER. The co-presence of Nafion and CB further enhances the HER activity, while CB alone does not add any significant beneficial effect for the CO_2RR (Fig. 5b). Based on the above analysis, it is considered unfavorable to fabricate electrodes with Nafion addition, and it is even more disadvantageous taking into account the high price of commercially available Nafion solution. PANI is an ionomer itself and can act as an ionic conductor. It also shows great affinity for the GDL substrate without a binder. Hence, it is encouraging that the PANI-based electrodes can be fabricated without any additives.

3.3 Electrochemical performances of various metal-doped PANI samples

The catalytic properties of EB-, Mn-, Cu-, Sn-, and Fe-PANI binder-free electrodes were investigated at − 0.79 V and − 0.99 V. Fe-PANI shows a FE_{H2} of 100%, even though the highest current densities of 4.9 and 8.8 mA cm^{-2} are obtained at − 0.79 and − 0.99 V, respectively (Figure S4 and S5). Figure S6a compares the selectivity of EB-, Mn-, Cu- and Sn-PANI for the CO_2RR at − 0.79 V. It is noticed that PANI alone shows a FE of 2.8% for HCOOH formation. The FE_{HCOOH} is enhanced to about 9.1% for Cu- and Sn-PANI. CO is observed on all three metal-doped PANI electrodes, with FE_{CO} values of 2.5–7.3%. The CO_2RR activity of EB-PANI electrode is significantly enhanced with Cu and Sn-doping, as evidenced by higher current densities for the CO and HCOOH production (Figure S6b). This outcome is in good agreement with the cyclic voltammetry and electrochemical impedance spectroscopy analysis (Figure S7 and S8). Doping of PANI with Fe ions leads to the highest electrode activity, while it results in no selectivity for the CO_2RR, as evidenced by a much lower charge transfer resistance in N_2-purged electrolyte than in the CO_2-saturated one at the same potential. In contrast, the PANI doped with Cu or Sn ions shows enhancement not only on the electrode activity, but also on the CO_2RR selectivity, as evidenced by the charge transfer resistance values obtained in CO_2-saturated electrolyte, which are similar or lower with respect to those obtained in N_2-purged solution [12].

Detailed analysis has been performed at − 0.99 V and shown in Fig. 6. As at − 0.79 V, the EB-PANI shows a selectivity only for HCOOH formation with a FE of 3.6% at − 0.99 V (Fig. 6a). While all Mn, Cu and Sn dopants

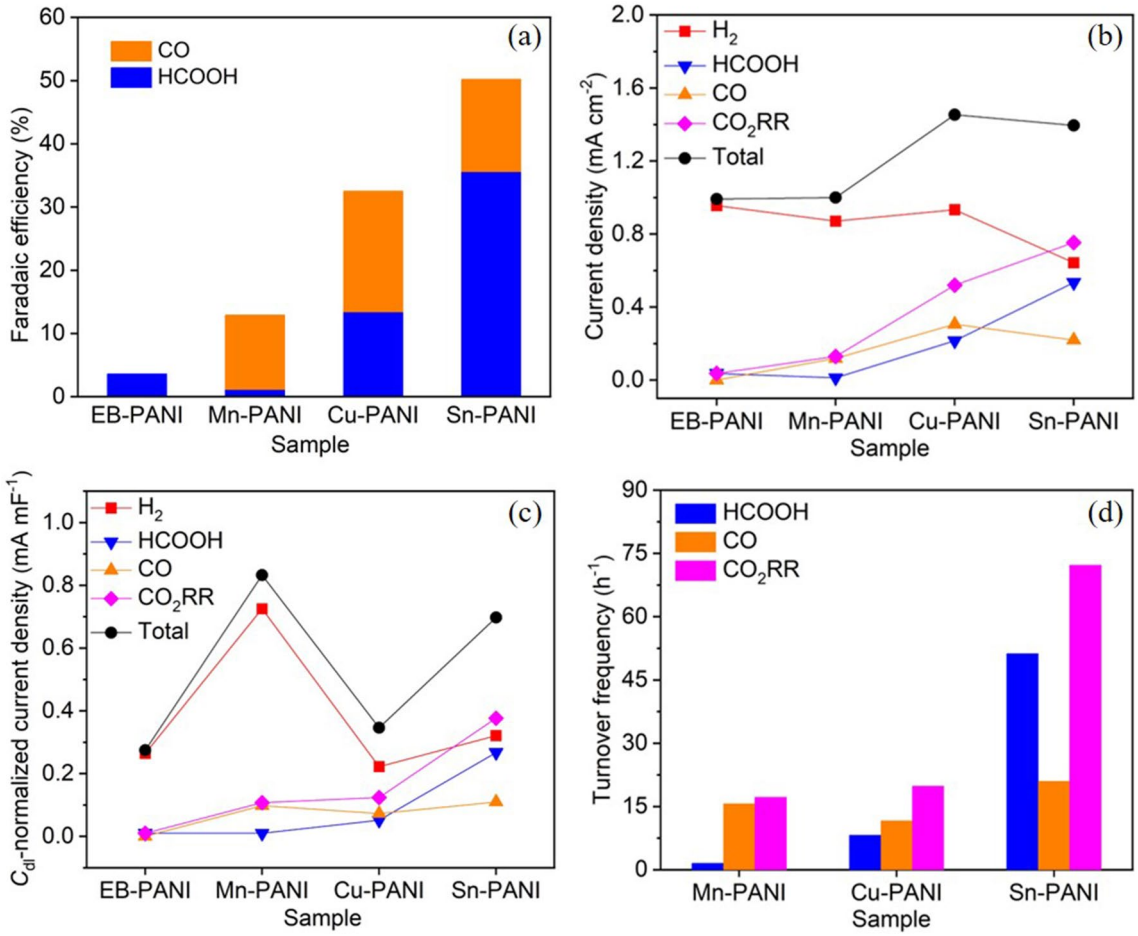

Fig. 6 CO_2RR on various electrodes in CO_2-saturated 0.1 M $KHCO_3$ electrolyte at − 0.99 V: **a** Faradic efficiencies for CO_2RR products, **b** partial current densities, **c** double-layer capacitance-normalized partial current densities and **d** turnover frequency for CO and HCOOH products

lead to a significant enhancement in the CO_2RR selectivity, the individual selectivity for CO or HCOOH formation is distinct. The Mn-PANI achieves a FE_{CO} of 11.8% and a small FE_{HCOOH} of 1.1%. The Cu-PANI enhances both the CO and HCOOH formation, with FE_{CO} and FE_{HCOOH} values of 19.1% and 13.4%, respectively. The Sn-PANI shows a significant increase in the FE_{HCOOH} (35.6%) and a modest FE_{CO} of 14.6%. Concisely, Mn-PANI is more selective for the CO and Sn-PANI is more selective for the HCOOH, while Cu-PANI produces CO and HCOOH almost equally. Figure 6b shows the electrode activity of various samples in terms of geometric current density. In general, the electrode activity of PANI can be enhanced by metal doping. The total current density on various electrodes follows the trend PANI ≈ Mn-PANI < Sn-PANI < Cu-PANI at − 0.99 V. The PANI electrode shows almost no partial current density for CO formation, while the metal doping significantly improves the CO formation, with a highest value of 0.3 mA cm^{-2} at the Cu-PANI electrode. HCOOH formation is remarkably enhanced on the Cu-PANI and Sn-PANI electrodes with respect to the PANI one. CO and HCOOH are the only detected CO_2RR products and the production rate of the C_1 products (CO + HCOOH) displays the trend Sn-PANI > Cu-PANI > Mn-PANI > PANI. These results demonstrate that the Cu- and Sn-doping have successfully modified the properties of PANI toward the CO_2RR.

The current normalized by the geometric surface area of the electrodes does not reflect the intrinsic activity of a catalyst. To evaluate the intrinsic activity of these materials, the current density is normalized by the electrochemically active surface area (ECSA). Since the ECSA is considered to be proportionally associated to the double-layer capacitance (C_{dl}), the intrinsic activity of various materials are compared by investigating the C_{dl}-normalized current densities at the electrodes. As detailed in the supporting information and shown in Figure S9, the C_{dl} values are found to be 3.6, 1.2, 4.3 and 2.0 mF cm^{-2} for EB-PANI, Mn-PANI, Cu-PANI and Sn-PANI electrodes, respectively. As shown in Fig. 6c, doping the PANI with a metal leads to an increase in the activity of the materials for reduction reactions, including

HER and CO_2RR. It is observed that the Mn-PANI shows the highest activity and the Cu-PANI has the lowest activity among the metal-doped samples. However, most of the activity of the Mn-PANI is attributed to the HER, leading to a comparable activity for the CO_2RR with respect to the Cu-PANI, and even a lower activity compared to the Sn-PANI sample. While the activity for CO formation is comparable at the three doped catalysts, the HCOOH formation is much more favorable on the Sn-PANI than on the others. It is also worth to note that the HER activity becomes inferior to CO_2RR for Sn-PANI, which is correlated with the low activity of p-group metals for the HER [42]. Figure 6d compares the CO and HCOOH formation rates normalized by the total metal atoms, that is turnover frequency (TOF, h^{-1}), at the three metal-doped PANI electrodes. It is evident that Sn-PANI outperforms the other counterparts with a higher atom efficiency for both CO and HCOOH formation. The TOF value is comparable with reported results for similar metal single-atom materials [43] and definitely higher than the bulk and nanostructured Sn-based catalysts [44], implying the good utilization efficiency of metal in the Sn-PANI complex.

The stability of Sn-PANI has further been investigated over 10-h CO_2 electrolysis at − 0.99 V, as shown in Fig. 7. The selectivity for CO and HCOOH formation remains quasi-stationary during the test (orange and blue squares, respectively), while the FE_{H2} firstly increases and then reaches a plateau (red squares). Surprisingly, the electrode activity displays a continuous growth over time (green line, current density), which could be attributed to the activation of the catalyst or the deeper wetness of the electrode. Since the selectivity is not notably changed, it is supposed that the characteristic of the catalyst is not changed either. Hence, the increase of current density is probably due to the increase

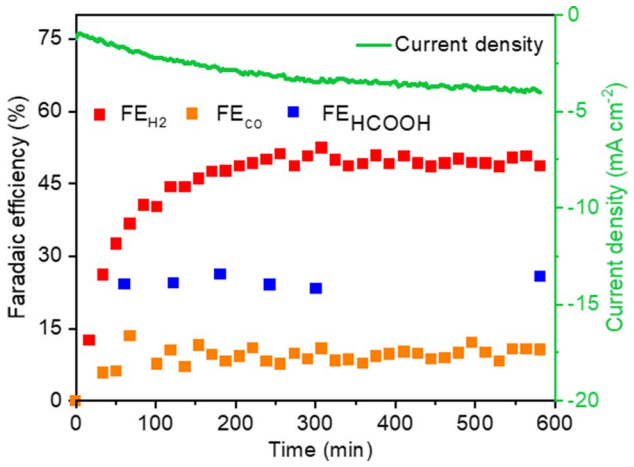

Fig. 7 Long-term test of Sn-PANI electrode. Faradaic efficiency and total current density as function of time in aqueous CO_2-saturated 0.1 M $KHCO_3$ solution at − 0.99 V

of the electrode wettability that leads to higher accessibility of active sites in the electrode [45]. Further investigation is needed to concretely elucidate this point. However, it is considered a positive aspect, since the CO_2RR rate is two-fold enhanced during 10-h operation.

4 Conclusions

In summary, the investigation of the electrode composition evidences the interesting propriety of PANI-based materials to be employed without any binder or ionic conductor, thus dramatically lowering the price and simplifying the process of the electrode preparation. The binder-free electrode shows good mechanical stability and higher selectivity for the CO_2RR with respect to the ones fabricated with Nafion binder. It is highlighted that an easy and novel process has been employed to anchor metal cations on PANI, resulting in new active sites for the CO_2RR. The metal cations of Mn, Cu, Sn and Fe have been investigated and show distinct characteristics, indicating the high tunability of the metal-PANI complexes. Sn-PANI outperforms the other samples and exhibits good selectivity, activity and durability for the CO_2RR, implying its good potential to be implemented in real devices. To the best of our knowledge, the Sn-PANI is synthesized and studied as electrocatalyst for the first time and its encouraging performance implies the good potential of exploring this material for the CO_2RR as well as other challenging electrochemical reactions.

Supplementary Information The online version contains supplementary material available at https://doi.org/10.1007/s10800-021-01585-7.

Author contributions The manuscript was written through contributions of all authors. All authors have given approval to the final version of the manuscript.

Funding Open access funding provided by Istituto Italiano di Tecnologia within the CRUI-CARE Agreement. This research did not receive any specific grant from funding agencies in the public, commercial, or not-for-profit sectors.

Declarations

Conflict of interest All authors declare that they have no conflict of interest.

References

1. Gao W, Liang S, Wang R, Jiang Q, Zhang Y, Zheng Q, Xie B, Toe C, Zhu X, Wang J, Huang L, Gao Y, Wang Z, Jo C, Wang Q, Wang L, Liu Y, Louis B, Scott J, Roger AC, Amal R, He H, Park S (2020) Industrial carbon dioxide capture and utilization: state of the art and future challenges. Chem Soc Rev 49:8584–8686. https://doi.org/10.1039/D0CS00025F
2. Xiao C, Lu BA, Xue P, Tian N, Zhou ZY, Lin X, Lin WF, Sun SG (2020) High-index-facet- and high-surface-energy nanocrystals of metals and metal oxides as highly efficient catalysts. Joule 4(12):2562–2598. https://doi.org/10.1016/j.joule.2020.10.002
3. Li CW, Kanan MW (2012) CO_2 reduction at low overpotential on Cu electrodes resulting from the reduction of thick Cu2O films. J Am Chem Soc 134(17):7231–7234. https://doi.org/10.1021/ja3010978
4. Zeng J, Bejtka K, Di Martino G, Sacco A, Castellino M, Re Fiorentin M, Risplendi F, Farkhondehfal MA, Hernández S, Cicero G, Pirri CF, Chiodoni A (2020) Microwave-assisted synthesis of copper-based electrocatalysts for converting carbon dioxide to tunable syngas. ChemElectroChem 7(1):229–238. https://doi.org/10.1002/celc.201901730
5. Chen Y, Fan Z, Wang J, Ling C, Niu W, Huang Z, Liu G, Chen B, Lai Z, Liu X, Li B, Zong Y, Gu L, Wang J, Wang X, Zhang H (2020) Ethylene selectivity in electrocatalytic CO_2 reduction on Cu nanomaterials: a crystal phase-dependent study. J Am Chem Soc 142(29):12760–12766. https://doi.org/10.1021/jacs.0c04981
6. Hsieh YC, Senanayake SD, Zhang Y, Xu W, Polyansky DE (2015) Effect of chloride anions on the synthesis and enhanced catalytic activity of silver nanocoral electrodes for CO_2 electroreduction. ACS Catal 5(9):5349–5356. https://doi.org/10.1021/acscatal.5b01235
7. Rosen J, Hutchings GS, Lu Q, Forest RV, Moore A, Jiao F (2015) Electrodeposited Zn dendrites with enhanced CO selectivity for electrocatalytic CO_2 reduction. ACS Catal 5(8):4586–4591. https://doi.org/10.1021/acscatal.5b00922
8. Zhao S, Jin R, Jin R (2018) Opportunities and challenges in CO_2 reduction by gold- and silver-based electrocatalysts: from bulk metals to nanoparticles and atomically precise nanoclusters. ACS Energy Lett 3(2):452–462. https://doi.org/10.1021/acsenergylett.7b01104
9. Rasul S, Pugnant A, Xiang H, Fontmorin JM, Yu EH (2019) Low cost and efficient alloy electrocatalysts for CO_2 reduction to formate. J CO2 Util 32:1–10. https://doi.org/10.1016/j.jcou.2019.03.016
10. Vickers JW, Alfonso D, Kauffman DR (2017) Electrochemical carbon dioxide reduction at nanostructured gold, copper, and alloy materials. Energy Technol 5(6):775–795. https://doi.org/10.1002/ente.201600580
11. Ju W, Zeng J, Bejtka K, Ma H, Rentsch D, Castellino M, Sacco A, Pirri CF, Battaglia C (2019) Sn-decorated Cu for selective electrochemical CO_2 to CO conversion: precision architecture beyond composition design. ACS Appl Energy Mater 2(1):867–872. https://doi.org/10.1021/acsaem.8b01944
12. Zeng J, Bejtka K, Ju W, Castellino M, Chiodoni A, Sacco A, Farkhondehfal MA, Hernández S, Rentsch D, Battaglia C, Pirri CF (2018) Advanced Cu–Sn foam for selectively converting CO_2 to CO in aqueous solution. Appl Catal B Environ 236:475–482. https://doi.org/10.1016/j.apcatb.2018.05.056
13. Deloitte Sustainability, British Geological Survey, Bureau de Recherches Géologiques et Minières, Netherlands Organisation for Applied Scientific Research (2017) Study on the review of the list of Critical Raw Materials- Criticality Assessments. Publications Office of the European Union, Luxembourg, ISBN 978-92-79-47937-3. https://doi.org/10.2873/876644
14. Han L, Song S, Liu M, Yao S, Liang Z, Cheng H, Ren Z, Liu W, Lin R, Qi G, Liu X, Wu Q, Luo J, Xin HL (2020) Stable and efficient single-atom Zn catalyst for CO_2 reduction to CH_4. J Am Chem Soc 142(29):12563–12567. https://doi.org/10.1021/jacs.9b12111
15. Nguyen TN, Salehi M, Le QV, Seifitokaldani A, Dinh CT (2020) Fundamentals of electrochemical CO_2 reduction on single-metal-atom catalysts. ACS Catal 10(17):10068–10095. https://doi.org/10.1021/acscatal.0c02643
16. Li M, Wang H, Luo W, Sherrell PC, Chen J, Yang J (2020) Heterogeneous single-atom catalysts for electrochemical CO_2 reduction reaction. Adv Mater 32(34):2001848. https://doi.org/10.1002/adma.202001848
17. Ghosh AC, Duboc C, Gennari M (2020) Synergy between metals for small molecule activation: enzymes and bio-inspired complexes. Coord Chem Rev 428:213606. https://doi.org/10.1016/j.ccr.2020.213606
18. Torbensen K, Boudy B, Joulié D, Wolff NV, Robert M (2020) Emergence of CO_2 electrolyzers including supported molecular catalysts. Curr Opin Electrochem 24:49–55. https://doi.org/10.1016/j.coelec.2020.07.001
19. Francke R, Schille B, Roemelt M (2018) Homogeneously catalyzed electroreduction of carbon dioxide—methods, mechanisms, and catalysts. Chem Rev 118(9):4631–4701. https://doi.org/10.1021/acs.chemrev.7b00459
20. Zheng W, Nayak S, Yuan W, Zeng Z, Hong X, Vincent KA, Tsang SCE (2016) A tunable metal-polyaniline interface for efficient carbon dioxide electro-reduction to formic acid and methanol in aqueous solution. Chem Commun 52(96):13901–13904. https://doi.org/10.1039/C6CC07212G
21. Wei X, Yin Z, Lyu K, Li Z, Gong J, Wang G, Xiao L, Lu J, Zhuang L (2020) Highly selective reduction of CO_2 to C_{2+} hydrocarbons at Cu/polyaniline interfaces. ACS Catal 10(7):4103–4111. https://doi.org/10.1021/acscatal.0c00049
22. Varela AS, Ju W, Bagger A, Franco P, Rossmeisl J, Strasser P (2019) Electrochemical reduction of CO_2 on metal-nitrogen-doped carbon catalysts. ACS Catal 9(8):7270–7284. https://doi.org/10.1021/acscatal.9b01405
23. Varela AS, Kroschel M, Leonard ND, Ju W, Steinberg J, Bagger A, Rossmeisl J, Strasser P (2018) PH effects on the selectivity of the electrocatalytic CO_2 reduction on graphene-embedded Fe–N–C motifs: bridging concepts between molecular homogeneous and solid-state heterogeneous catalysis. ACS Energy Lett 3(4):812–817. https://doi.org/10.1021/acsenergylett.8b00273
24. Bocchini S, Chiolerio A, Porro S, Accardo D, Garino N, Bejtka K, Perrone D, Pirri CF (2013) Synthesis of polyaniline-based inks, doping thereof and test device printing towards electronic applications. J Mater Chem C 1(33):5101–5109. https://doi.org/10.1039/c3tc30764f
25. Chiolerio A, Bocchini S, Crepaldi M, Bejtka K, Pirri CF (2017) Bridging electrochemical and electron devices: fast resistive switching based on polyaniline from one pot synthesis using $FeCl_3$ as oxidant and Co-doping agent. Synth Met 229:72–81. https://doi.org/10.1016/j.synthmet.2017.05.001
26. Shirley DA (1972) High-resolution X-ray photoemission spectrum of the valence bands of gold. Phys Rev B 5:4709. https://doi.org/10.1103/PhysRevB.5.4709
27. Bocchini S, Castellino M, Della Pina C, Rajan K, Falletta E, Chiolerio A (2018) Inkjet printed doped polyaniline: navigating

through physics and chemistry for the next generation devices. Appl Surf Sci 456:246–258. https://doi.org/10.1016/j.apsusc.2018.06.003
28. Kumar SN, Gaillard F, Bouyssoux G, Sartre A (1990) High-resolution XPS studies of electrochemically synthesized conducting polyaniline films. Synth Met 36(1):111–127. https://doi.org/10.1016/0379-6779(90)90240-L
29. Vasquez RP (1993) CuCl by XPS. Surf Sci Spectra 2(2):138–143. https://doi.org/10.1116/1.1247732
30. Biesinger MC (2017) Advanced analysis of copper X-ray photoelectron spectra. Surf Interface Anal 49(13):1325–1334. https://doi.org/10.1002/sia.6239
31. Xu H, Zhang J, Chen Y, Lu H, Zhuang J (2014) Electrochemical polymerization of polyaniline doped with Cu^{2+} as the electrode material for electrochemical supercapacitors. RSC Adv 4(11):5547–5552. https://doi.org/10.1039/c3ra45794j
32. Vasnin S, Geanangel RA (1989) Adducts of Tin(II) chloride with imidazole and methylimidazoles. Inorganica Chim Acta 160(2):167–170. https://doi.org/10.1016/S0020-1693(00)80581-2
33. Nesbitt HW, Banerjee D (1998) Interpretation of XPS Mn(2p) spectra of Mn oxyhydroxides and constraints on the mechanism of MnO_2 precipitation. Am Mineral 83:305–315. https://doi.org/10.2138/am-1998-3-414
34. Biesinger MC, Payne BP, Grosvenor AP, Lau LWM, Gerson AR, Smart RSC (2011) Resolving surface chemical states in XPS analysis of first row transition metals, oxides and hydroxides: Cr, Mn, Fe, Co and Ni. Appl Surf Sci 257(7):2717–2730. https://doi.org/10.1016/j.apsusc.2010.10.051
35. Grosvenor AP, Kobe BA, Biesinger MC, McIntyre NS (2004) Investigation of multiplet splitting of Fe 2p XPS spectra and bonding in iron compounds. Surf Interface Anal 36(12):1564–1574. https://doi.org/10.1002/sia.1984
36. Xu H, Wu J, Li C, Zhang J, Liu J (2015) Investigation of polyaniline films doped with Fe^{3+} as the electrode material for electrochemical supercapacitors. Electrochim Acta 165:14–21. https://doi.org/10.1016/j.electacta.2015.01.224
37. Yoon SB, Yoon EH, Kim KB (2011) Electrochemical properties of leucoemeraldine, emeraldine, and pernigraniline forms of polyaniline/multi-wall carbon nanotube nanocomposites for supercapacitor applications. J Power Sources 196(24):10791–10797. https://doi.org/10.1016/j.jpowsour.2011.08.107
38. Gul S, Shah AUHA, Bilal S (2013) Synthesis and characterization of processable polyaniline salts. J Phys: Conf Ser 439:012002. https://doi.org/10.1088/1742-6596/439/1/012002
39. Izumi CMS, Rodrigues DC, Pelaes LAG, Da Costa Ferreira AM, Temperini MLA (2016) Influence of different copper(II) salts on the oxidation and doping reactions of emeraldine base polyaniline. Vib Spectrosc 87:129–136. https://doi.org/10.1016/j.vibspec.2016.09.019
40. Jhong HRQ, Brushett FR, Kenis PJA (2013) The effects of catalyst layer deposition methodology on electrode performance. Adv Energy Mater 3(5):589–599. https://doi.org/10.1002/aenm.201200759
41. Ott S, Orfanidi A, Schmies H, Anke B, Nong HN, Hübner J, Gernert U, Gliech M, Lerch M, Strasser P (2020) Ionomer distribution control in porous carbon-supported catalyst layers for high-power and low Pt-loaded proton exchange membrane fuel cells. Nat Mater 19(1):77–85. https://doi.org/10.1038/s41563-019-0487-0
42. Bejtka K, Zeng J, Sacco A, Castellino M, Hernández S, Farkhondehfal MA, Savino U, Ansaloni S, Pirri CF, Chiodoni A (2019) Chainlike mesoporous SnO_2 as a well-performing catalyst for electrochemical CO_2 reduction. ACS Appl Energy Mater 2(5):3081–3091. https://doi.org/10.1021/acsaem.8b02048
43. Ju W, Bagger A, Hao GP, Varela AS, Sinev I, Bon V, Roldan Cuenya B, Kaskel S, Rossmeisl J, Strasser P (2017) Understanding activity and selectivity of metal-nitrogen-doped carbon catalysts for electrochemical reduction of CO_2. Nat Commun 8(1):1–9. https://doi.org/10.1038/s41467-017-01035-z
44. Zhao S, Li S, Guo T, Zhang S, Wang J, Wu Y, Chen Y (2019) Advances in Sn-based catalysts for electrochemical CO_2 reduction. Nano-Micro Lett 11:62. https://doi.org/10.1007/s40820-019-0293-x
45. Kolyagin GA, Kornienko VL (2018) Effect of electric current on the wettability of carbon-containing gas diffusion electrodes by aqueous solutions and the change in their capacitance characteristics. Russ J Electrochem 54(12):1288–1293. https://doi.org/10.1134/S1023193518130220

Authors and Affiliations

Daniele Sassone[1,2] · Juqin Zeng[1] · Marco Fontana[1] · Adriano Sacco[1] · M. Amin Farkhondehfal[1] · Monica Periolatto[2] · Candido F. Pirri[1,2] · Sergio Bocchini[1]

[1] Center for Sustainable Future Technologies (CSFT)@ Polito, Istituto Italiano Di Tecnologia, Via Livorno 60, 10144 Torino, Italy

[2] Department of Applied Science and Technology—DISAT, Politecnico Di Torino, Corso Duca degli Abruzzi 24, 10129 Torino, Italy